School of Traditional Chinese Medicine[1], School of Medicine and Chemical Engineering[2], Guangdong Pharmaceutical University, Guangzhou, China

Lipid-coated mesoporous silica nanoparticles of hydroxycamptothecin for sustained release and cancer therapy

Xiaofang Liu[1], Musheng Li[1], Wanwen Yuan[1], Yuan Liu[1], Ying Wang[2,*], Yan Wang[1,*]

Received March 30, 2018, accepted June 27, 2018

**Corresponding authors: Ying Wang, School of Medicine and Chemical Engineering, Guangdong Pharmaceutical University, Guangzhou, 510006, China*
1248322680@qq.com
Yan Wang, School of Traditional Chinese Medicine, Guangdong Pharmaceutical University, Guangzhou, 510006, China
gdpuwy@126.com

Pharmazie 73: 447-453 (2018) *doi: 10.1691/ph.2018.8065*

Lipids with galactosylceramide-coated mesoporous silica nanoparticles were formulated in this study as a new strategy for the delivery of the poorly-soluble anticancer drug, hydroxycamptothecine. To improve drug loading, the mesoporous silica nanoparticle formulations and one of its preparation step-removal of cetyltrimethylammonium bromide were optimized under different conditions. The optimization produced uniform MSN with a hexagonal pore structure, surface area of 1131.48 $m^2 \cdot g^{-1}$, and HCPT drug loading of up to 29.94%. The surface of HCPT loaded with MSN was lipid-coated (HCPT-GC-LMSN) using a simple lipid film hydration method, optimized using the central composite design-response surface methodology, and then galactoseceramide was added to the lipid. The prepared HCPT-GC-LMSN was characterized using transmission electron microscopy, and particle size measurement indicated successful coating with an approximately 25 nm-thick lipid membrane. The *in vitro* cumulative release of HCPT-GC-LMSN was 48.82% within 36 h under a simulated tumor environment, showing sustained release properties. The cell-counting kit, (CCK)-8 cell viability test showed that HCPT-GC-LMSN had stronger inhibitory effects on hepatocellular carcinoma cells with a half-maximal inhibitory value of 7.13 μg/mL after 72 h, which was 2.97 times that than of HCPT. This formulated lipid with galactosylceramide-coated MSN could provide an effective strategy for delivering poorly-soluble anticancer drugs.

1. Introduction

Various materials have been used as drug vehicles, such as inorganic nanoparticles, which have become a new generation of drug delivery vehicles in nanomedicine. Mesoporous silica nanoparticles (MSN) are particularly attractive in this field (Yanes and Tamanoi 2012) because they have several outstanding features such as a large surface area, uniform and tailorable pore sizes, and controllable particle sizes and shapes, as well as chemically inert, dual-functional, and easily functionalized surfaces (Gao et al. 2011; Li et al. 2012; Slowing et al. 2007; Vallet-Regí et al. 2007). All these features enhance the control of drug loading and release.

Drugs and other components can be loaded by adsorption or capillary filling, and the release profiles can be adjusted by modulating the pore size and pore surface chemistry. An important advantage of MSN is that they overcome the problem of insolubility of numerous anticancer drugs (Liong et al. 2008; Lu et al. 2010). The loading capacities of MSN have been reported to normally vary from 10% to 34% (Qu et al. 2006) or up to 60% (Heikkilä et al. 2007) in extreme cases. Furthermore, owing to high biocompatibility, MSN is promising for various biomedical applications such as drug delivery vehicles, gene transfection reagents, cell markers, and molecule carriers (Hsiao et al. 2008, Liu et al. 2008; Lu et al. 2010).

As a new technology for the development of drug delivery vehicles, the lipid-coated MSN (LMSN) is considered a promising carrier for drug delivery by combining the advantages of liposomes and MSN (Mudakaci et al. 2014; Qiu et al. 2017; Song et al. 2017). Furthermore, with their core structure, MSN can support a mechanically stable lipid membrane. Moreover, the lipid membrane, with high biocompatibility and pH sensitivity, can increase the cellular uptake of drugs and control drug release under acidic conditions. Compared to other nanoparticle delivery systems such as liposomes, LMSN is simple and stable (Teng et al. 2013) and has the advantage of liposomes with low toxicity and immunogenicity and the advantage of MSN by controlling drug loading and release (Liu et al. 2009). Because of the specific binding capacity of galactose residues to asialin receptors on mammalian liver cells, galactosylceramide (GC), which has galactose residues actively accumulates in the liver (Lee et al. 2012).

Camptothecin (CPT), an alkaloid isolated from the Chinese plant *Camptotheca acuminata*, is a potent broad-spectrum anticancer agent (Jaxel et al. 1989) that kills tumor cells by targeting the nuclear enzyme, topoisomerase I, and inhibiting the relegation of the cleaved DNA strand (Wang et al. 2009). A CPT analog, hydroxycamptothecin (HCPT), which is more potent and less toxic (Fu et al. 2006), demonstrated strong antitumor activity against hepatoma, head and neck tumors, as well as gastric, lung, ovarian, breast, and pancreatic carcinomas (Pu et al. 2009). However, HCPT has poor water solubility, which is a major challenge to its clinical application. In an alkaline environment, the lactone ring of HCPT can be opened to enhance the water solubility, but this decreases activity and increases toxicity (O'Leary and Muggia 1998) such as myelosuppression, hemorrhagic cystitis, vomiting, nausea, and dermatitis (Zhao et al. 2012). To overcome these limitations, many different delivery systems have been developed including nanocrystallites (Wei et al. 2010) micelles (Lin et al. 2015) and nanoparticles (Dai et al.,2015; Fan et al. 2016; Yang et al. 2014).

In the present study, lipid with galactosylceramide-coated MSN was constructed, combining the advantages of liposome and MSN to control drug loading and release. We hope that it will provide a novel strategy for the delivery of poorly soluble anti-cancer drugs.

2. Investigations, results and discussion

2.1. Synthesis and optimization of MSN

In the first step, MSN was prepared using the modified Stöber method, and the best formulation was determined using particle size and potential as evaluation indices in the single factor study (Table 1). The results showed that the MSN particle size changed when the factors were varied. It decreased with increasing CTAB concentration and temperature, as well as increasing TEOS and NaOH concentrations, while decreased first and then increased with the increase of ethanol consumption. This could be explained by the reaction underlying the modified Stöber method. The reaction process is mainly divided into two steps (Fig. 1). The first step is a hydrolysis reaction, in which a silicic acid monomer and alcohol are formed after TEOS hydrolysis. The second step is a condensation reaction between silicic acid monomers or a silicic acid monomer and TEOS, producing silicon oxide sol particles (Li et al. 2003).

As the reaction progresses, a spatial network structure is eventually formed. Moreover, the negatively charged sol particles are adsorbed onto the positively charged micellar surface formed by CTAB under Van der Waal's and electrostatic forces when the solution pH is suitable. Subsequently, the inorganic-organic complex micelles self-assemble to form nucleations and finally form the MSN by removal of CTAB using calcination or sol extraction methods. In this process, as the main reactant, the concentration of CTAB affects the structure and morphology of the MSN (Vittal et al. 2008). Increasing the CTAB concentration increased the number of micelles formed in the reaction system, and when other factors fixed, it meant that the average number of silicic acid monomers adsorbed on the surface of each micelle was relatively decreased, resulting in the shorten three-dimensional network chains. Cross-linking polymerization between short chains leads to a product with smaller particle sizes (Table 1, group 1, 2, 3). The concentration of CTAB required to form micelles also depended on the temperature, and there was a tendency to form rod-like micelles and not spherical MSN with larger particle size and even agglomeration at low temperature (Table 1, group 2, 10, 11).

Increasing the concentration of another major reactant, TEOS promoted hydrolysis, which formed more silicic acid monomers, leading to a larger particle size (Table 1, group 2, 4, 5). Both TEOS and OH- ions from NaOH affect the electrostatic adsorption between the micelles and the sol particles, resulting in the agglomeration of MSN (Vivero-Escoto et al. 2010) (Table 1, group 2, 6, 7). Ethanol, as a co-solvent, was one of the products of hydrolysis (Yamada and Yano 2006), which affected the solubility of CTAB in solution and, therefore, the appropriate amount of ethanol could make the MSN particle size small and homogeneous (Yano and Fukishima 2004) (Table 1, group 2, 8, 9).

In the second step, the solvent extraction method was used to remove the template agent CTAB, and the removal formulation was obtained using a single factor investigation with the specific surface area, pore volume, and pore size as the evaluation index (Table 2). MSN provided a good platform for loading the poorly soluble drug (Lu et al. 2010; Qu et al. 2006), and the drug loading capacity depended largely on the specific surface area. Therefore, we referred to numerous literature reports (Alvarez-Berríos and Vivero-Escoto 2016; Huang et al. 2017; Lv et al. 2017) and combined with our laboratory conditions, we decided to use solvent extraction to remove the template agent CTAB, and this is the first time the extraction efficiency of various of solvents has been evaluated. First, five extraction solvents were selected based on the literature references and laboratory conditions. The hydrochloric acid/ethanol showed the best removal ability for CTAB among the five solvents although they were all efficient.

Next, the effect of acid-alcohol ratio on the removal was examined, and the result showed that the specific surface area decreased with an increasing proportion of hydrochloric acid. Considering the poor effect of single ethanol on absolute extraction, we speculated that a certain percentage of acid alcohol solvent could dissolve CTAB in the pores. However, the increasing proportion of the acid resulted in a solvent mix with low solubility for CTAB, which was even close to a saturated state. Therefore, the mixed solvent could not be dissolved CTAB of materials any further, leading to a worse removal effect. Finally, we found that the effect of removal was poor when the extraction time was prolonged, and the temperature was too high, which was also possibly caused by the reduction of ethanol.

Therefore, based on the above two steps, MSN was prepared and then characterized. The MSN particles were spherical with a uniform distribution (Fig. 2 A) observed using SEM. The particle size was 270±11.4 nm, and the potential was -44.29±1.9 mV

Table 1: Selected formulations for MSN for synthesis

Group	CTAB conc. (mol/L)	TEOS conc. (mol/L)	NaOH conc. (mol/L)	Alcohol/ water ratio (v/v)	Temperature (°C)	Particles size (nm)	PDI	Zeta-potential (mV)
1	0.0056	0.0512	0.0118	1:8	80	359±10.2	0.19±0.09	-40.7±2.5
2	0.0061	0.0512	0.0118	1:8	80	270±11.4	0.16±0.10	-44.3±1.9
3	0.0065	0.0512	0.0118	1:8	80	225±10.5	0.15±0.09	-45.9±2.1
4	0.0061	0.0412	0.0118	1:8	80	241±10.3	0.18±0.11	-40.1±1.9
5	0.0061	0.0617	0.0118	1:8	80	401±11.6	0.21±0.14	-42.0±2.2
6	0.0061	0.0512	0.0088	1:8	80	236±10.6	0.19±0.10	-41.8±2.1
7	0.0061	0.0512	0.0148	1:8	80	345±10.3	0.22±0.15	-40.3±1.8
8	0.0061	0.0512	0.0118	1:12	80	1228±13.6	0.52±0.16	-4.4±1.9
9	0.0061	0.0512	0.0118	1:6	80	585±12.1	0.28±0.09	-4.4±2.3
10	0.0061	0.0512	0.0118	1:8	40	1718±13.9	0.80±0.18	-2.7±2.5
11	0.0061	0.0512	0.0118	1:8	60	406±11.5	0.22±0.11	-38.6±2.1

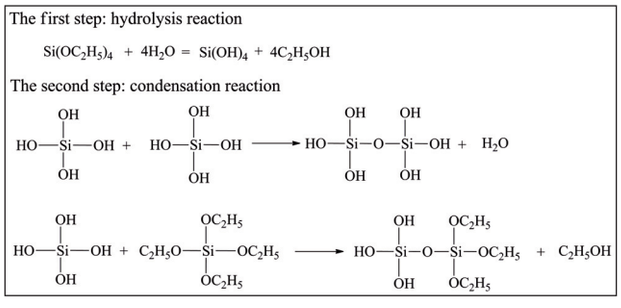

Fig. 1: Main reaction of the Stöber method.

Table 2: Selected formulations for the removal of CTAB

Group	Solvent types	Acid/ alcohol ratio	Time(h)	Temperature (°C)	Specific surface area ($m^2 \cdot g^{-1}$)	Pore volume ($cm^3 \cdot g^{-1}$)	Pore size (nm)
1	Hydrochloric acid/Methanol	5.3%	6	80	852.81	0.74	3.26
2	Acetic acid/Anhydrous ethanol	5.3%	6	80	988.53	0.84	3.28
3	Hydrochloric acid/Anhydrous ethanol	5.3%	6	80	1131.48	1.30	3.60
4	Ammonium nitrate/Anhydrous ethanol	5.3%	6	80	766.54	0.44	3.22
5	Anhydrous ethanol	5.3%	6	80	209.11	0.32	4.19
6	Hydrochloric acid/Anhydrous ethanol	15.0%	6	80	799.69	0.41	4.15
7	Hydrochloric acid/Anhydrous ethanol	20.0%	6	80	831.44	0.59	3.26
8	Hydrochloric acid/Anhydrous ethanol	5.3%	4	80	886.86	0.53	3.54
9	Hydrochloric acid/Anhydrous ethanol	5.3%	8	80	835.79	0.52	3.43
10	Hydrochloric acid/Anhydrous ethanol	5.3%	6	70	827.60	0.48	3.16
11	Hydrochloric acid/Anhydrous ethanol	5.3%	6	90	959.47	0.61	3.35

(n = 3, Fig. 2 B) detected using laser particle size analyzer. The morphological structure of the MSN was observed using TEM to show the homogeneously spherical and an ordered hexagonal pore structure arranged radially from the inside and to the outside (Fig. 2 C). The pore properties of MSN were confirmed using XRD and nitrogen adsorption-desorption characterizations.

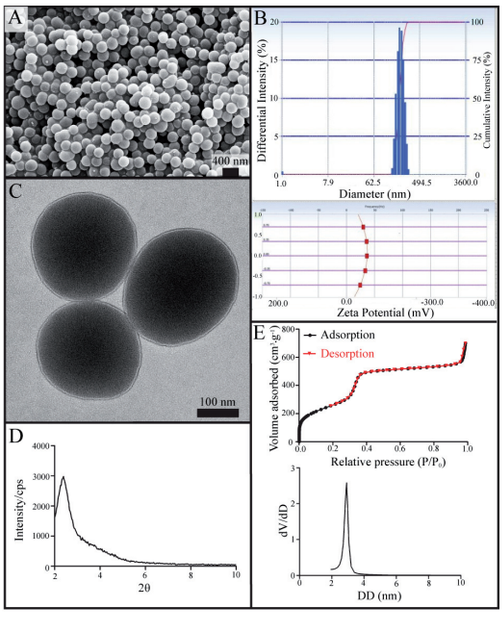

Fig. 2: Characterization of MSN (A: SEM images of prepared MSN with spherical morphology; B: Images showing the particle size (270±11.4 nm) and zeta-potential distribution (44.29±1.9 mV) of prepared MSN (n=3, mean±SD); C: TEM images showing the spherical morphology and ordered hexagonal pore structure of the prepared MSN; D: XRD images showing a diffraction peak at 2-3° of 2θ angle; E: nitrogen adsorption-desorption isotherm plots and pore size distribution curve showing 1131.48 $m^2 \bullet g^{-1}$ of surface area, 1.30 $cm^3 \bullet g^{-1}$ of pore volume, and 3.6 nm of pore size).

The characterization of XRD was consistent with that of the TEM, which showed a diffraction peak at a 2θ angle in the range of 2-3° indicating that the prepared MSN had a hexagonal mesoporous structure (Fig. 2 D). The nitrogen adsorption-desorption isotherm could be classified as type IV isotherm according to the International Union of Pure and Applied Chemistry (IUPAC) nomenclature (Sing 1985). The specific surface area of the synthesized MSN was 1131.48 $m^2 \cdot g^{-1}$, with a measured mesoporous volume of 1.30 $cm^3 \cdot g^{-1}$ and a narrow distribution for the pore size centered at 3.6 nm (Fig. 2 E). All the characterization results showed that the MSN samples prepared according to the optimized formulation had good morphology and ordered hexagonal mesoporous properties.

2.2. Preparation of HCPT-MSN

MSN was loaded with HCPT using a solvent adsorption method and the effect of the HCPT/MSN ratio (1:1, 1:2, 1:3, and 1:5, w/w) on drug loading was investigated (Fig. 3). The results showed that the highest drug loading was obtained at an HCPT/MSN ratio of 1:1 and the drug loading decreased with increasing ratio of HCPT/MSN. To verify this process, three samples were prepared in parallel, and the drug loading capacity and relative SD (RSD) were calculated. The average drug loading capacity of the three samples was 29.94 % with 0.32 % RSD, indicating that the drug loading method was feasible and robust. Compared with other reported solvent extraction conditions (Alvarez-Berríos and Vivero-Escoto 2016; Huang et al. 2017; Lv et al. 2017), our optimized process achieved a greater specific surface area, as evidenced by the high drug loading efficiency of HCPT (29.94%), and was time-saving.

2.3. Preparation and optimization of HCPT-GC-LMSN

The lipid membrane was coated on the HCPT-MSN surface using a lipid film hydration method, and the condition was optimized using CCD-RSM. Compared with the traditional optimization methods

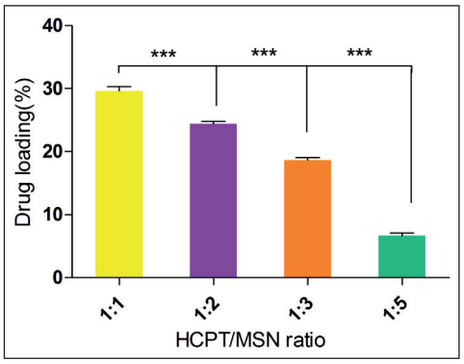

Fig. 3: Impact of different HCPT / MSN ratios on drug loading using solvent adsorption method (***P< 0.05).

such as orthogonal design, CCD-RSM is a method with higher accuracy that uses the nonlinear model to fit the experimental data and further optimize the formulation prescription (Dutta and Basu 2012; Huang et al. 2012). Therefore, based on the results of the previous preliminary experiments, four factors (cholesterol concentration, phospholipid concentration, HCPT-MSN concentration, and temperature) were selected, and a four-factor and five-level code table was obtained using CCD-RSM (Table 3). Then, the optimized experiments were carried out, and the data were analyzed using the Design-Expert 8.05 software (Table 4). The binary polynomial regression equation $Y= 29.15 -1.17X_1 + 2.45X_2 + 1.77X_3 + 0.87X_4 + 0.85X_1X_2 + 0.31X_1X_3 + 0.074X_1X_4 + 1.32X_2X_3 - 2.57X_2X_4 + 2.24X_3X_4 - 3.51X_1^2 - 4.62X_2^2 - 1.55X_3^2 + 2.15X_4^2$ (correlation coefficient $[R^2] = 0.9268$) was obtained using quadratic polynomial nonlinear regression, and $R^2 > 0.9$, indicating a good fitting degree and a positive correlation. Then, the graphs of the three-dimensional response surface and contour plots were constructed to study the effect of various factors according to the binomial equation fitting analysis. Response surface plots can be used to study surfaces and locate the optimal response to maximize EE (Qu et al. 2011). The above process produced optimal values of X_1, X_2, X_3, and X_4 at 0.6, 5, and 0.5 mg/mL and 45 °C, respectively, and the optimal EE was 46.63%. Finally, the best formulation was verified using three batches of samples, and the result showed that the deviation between the observed and expected values was < 5%, indicating that the optimized model had a positive predictive effect and high reliability (Table 5).

Preparation of LMSN is extremely time-consuming (Dengler et al. 2013; Teng et al. 2013; Tu et al. 2017), and requires preparing a liposomal suspension by rotary evaporation film, hydration, and then incubation with drug-loaded MSN for a period. In contrast, in this experiment, a simple, time-saving process for HCPT-LMSN was developed based on a direct lipid film hydration method without any subsequent incubation steps, and also was connected with GC, which specifically targets the liver. For HCPT-GC-LMSN, TEM characterization showed that the lipid membrane was coated on the surface successfully and the mesoporous structure disappeared. However, the HCPT-GC-LMSN was still spherical with uniform distribution compared to the MSN before coating (Fig. 4 A). The particle size of the HCPT-GC-LMSN increased to 294.75±10.5 nm (n = 3), and the thickness of lipid membrane was approximately 25 nm, as determined using a particle size analyzer (Fig. 4 B). The result of characterization confirmed that the lipid membrane was successfully coated on the HCPT-MSN surface.

Table 3: Prescription and the variable level of codes from CCD-RSM

Factor	Level				
	-2	-1	0	+1	+2
X_1 (mg/mL)	0.45	0.52	0.6	0.68	0.75
X_2 (mg/mL)	4	4.5	5	5.5	6
X_3 (mg/mL)	0.3	0.35	0.4	0.45	0.5
X_4 (°C)	30	33.75	37.5	41.25	45

Notes: X_1, the concentration of cholesterol; X_2, the concentration of phospholipid; X_3, the concentration of HCPT-MSN; X_4, temperature.

Table 4: CCD-RSM design results

	codes				Entrapment efficiency (%)
	X_1	X_2	X_3	X_4	
1	-1	-1	-1	-1	19.05
2	1	-1	-1	-1	15.39
3	-1	1	-1	-1	28.47
4	1	1	-1	-1	20.60
5	-1	-1	1	-1	15.31
6	1	-1	1	-1	13.36
7	-1	1	1	-1	28.57
8	1	1	1	-1	29.41
9	-1	-1	-1	1	19.89
10	1	-1	-1	1	16.07
11	-1	1	-1	1	16.62
12	1	1	-1	1	17.45
13	-1	-1	1	1	30.82
14	1	-1	1	1	21.40
15	-1	1	1	1	27.95
16	1	1	1	1	28.89
17	-2	0	0	0	15.73
18	2	0	0	0	13.70
19	0	-2	0	0	7.21
20	0	2	0	0	13.30
21	0	0	-2	0	22.50
22	0	0	2	0	22.62
23	0	0	0	-2	34.36
24	0	0	0	2	40.33
25	0	0	0	0	29.70
26	0	0	0	0	32.52
27	0	0	0	0	29.41
28	0	0	0	0	29.56
29	0	0	0	0	26.65
30	0	0	0	0	27.09

Notes: X_1, the concentration of cholesterol; X_2, the concentration of phospholipid; X_3, the concentration of HCPT-MSN; X_4, temperature.

Table 5: Verification results of the optimized condition

Sample	Expected value	Observed values	Deviation (%)
1		47.49	3.64
2	45.82	47.06	2.70
3		45.34	-1.05

2.4. In vitro drug release

The results of the in vitro drug release were shown in Fig. 5. After 36 h, the accumulative release degree of HCPT under normal body fluid environment (pH 7.4, 37±1 °C) reached 80.13 % (Curve line 1) while that of HCPT-GC-LMSN was only 33.81 %, but with a

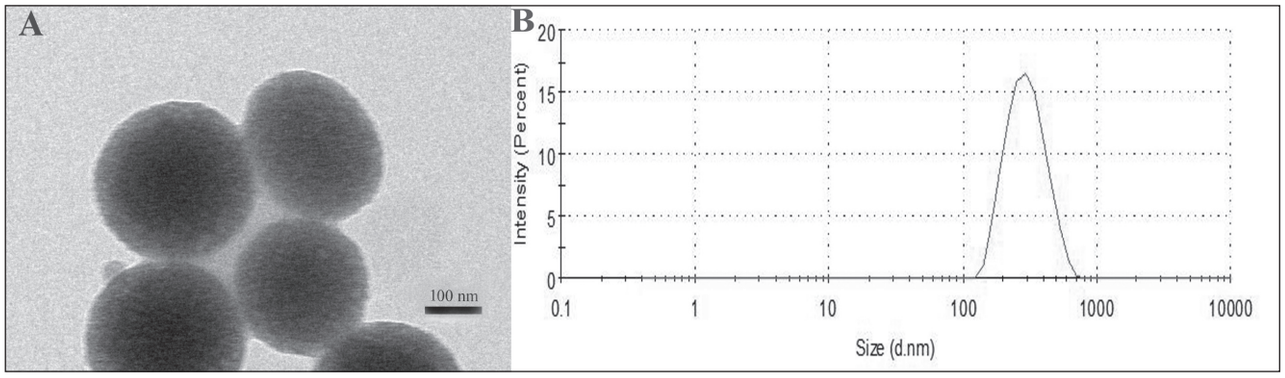

Fig. 4: Characterization of HCPT-GC-LMSN (A: TEM images of prepared HCPT-GC-LMSN with a 25-nm thickness of lipid membrane on the surface; B: particle size distribution images of prepared HCPT-GC-LMSN having a particle size of 294.75 ± 10.5 nm (n = 3, mean±SD)).

sustained increasing release trend (Curve line 3). This indicated that the HCPT-GC-LMSN had an advantage of sustained slow release. Similar to what is evident in line 3, the release of HCPT-GC-LMSN under the simulated tumor environment (Curve line 2) was faster with a accumulative release degree of 48.82% after 36 h. This occurred because the lipid membrane did not remain intact in the slightly acidic and hyperthermic tumor environment, thereby accelerating drug release (Wu et al. 2013). The above results might indicated that HCPT-GC-LMSN maintained a more complete structure in body fluids, which reduced the off-target drug release while accelerating that in tumor sites to improve efficacy.

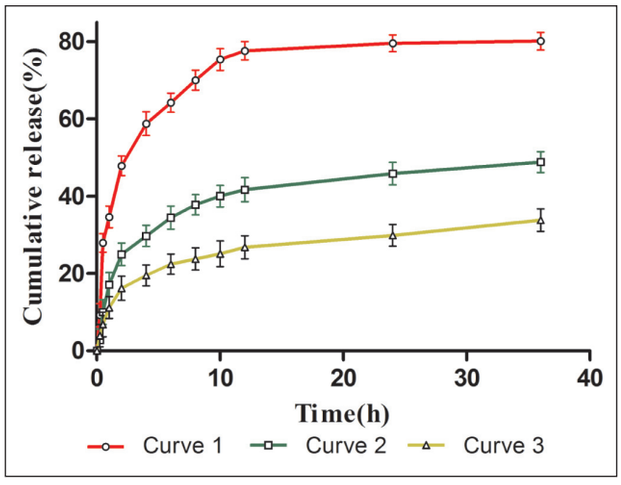

Fig. 5: Drug release lines of equal dose HCPT-GC-LMSN and HCPT (curve line 1: HCPT release in 1% SDS PBS (pH=7.4), 37±1 °C; curve line 2: HCPT-GC-LMSN release in 1% SDS PBS (pH=5.8), 42±1 °C; curve line 3: HCPT-GC-LMSN release in 1% SDS PBS (pH=7.4), 37±1 °C).

2.5. CCK-8 cell viability assay

The *in vitro* cell viability was evaluated in $HepG_2$ cells using the CCK-8 kit assay, and the results were illustrated in Fig. 6. After the two groups of cells were exposed to various concentrations of HCPT (2.5, 5, 10, 20, and 40 μg/mL), the cell viability was significantly decreased by HCPT in a concentration-dependent manner. Similarly, cells treated with the same concentration of HCPT for different times (24, 48, and 72 h) showed a time-dependent decrease in viability. Moreover, the cell viability following HCPT-GC-LMSN treatment was consistently lower than that with HCPT either at a low or high concentration or for long or short reaction times, indicating a stronger anticancer effect on $HepG_2$ cells. This occurred because the lipid membrane coated with HCPT-GC-LMSN was similar to the cell membrane, which has good biocompatibility and promoted the intracellular release of the drug. Following incubation with $HepG_2$ cells for 72 h, the IC_{50} of the HCPT-GC-LMSN was 2.405 μg/mL, which is 2.97 times than that of HCPT, also indicating strong inhibition. The results showed that GC-LMSN as a carrier could improve the inhibitory effect of HCPT on $HepG_2$ cell growth.

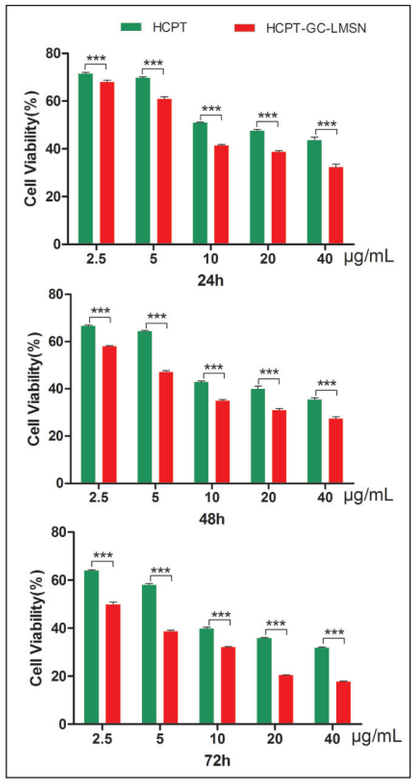

Fig. 6: Dose- and time-dependent effects of HCPT-GC-LMSN on HepG₂ cells under different concentrations and at different time periods, determined by CCK-8 kit (n = 3, mean±SD, ***P<0.001).

2.6. Conclusion

In this study, MSN formulations with a large specific surface area and loading capacity for insoluble drugs were prepared, and the conditions were optimized. HCPT-GC-LMSN was directly prepared using a lipid film hydration method by coating a lipid membrane onto the surface of the HCPT-MSN. In vitro release experiment and cell viability assay showed that HCPT-LMSN had a sustained release property and stronger inhibitory effect on $HepG_2$ cells than HCPT did. The method of formulating MSN coated with lipid and GC could provide a new strategy for improved delivery of insoluble anticancer drugs.

3. Experimental

3.1. Materials

HCPT (molecular weight [MW] = 364.35, purity ≥ 98%) was purchased from Nantong Feiyu Biological Technology Co., Ltd., (Jiangsu, China). Tetraethyl orthosilicate (TEOS) and cetyltrimethyl ammonium bromide (CTAB) were purchased from Sinopharm Chemical Reagent Co., Ltd., (Shanghai, China). The cell counting kit (CCK)-8 was purchased from Dojindo (Japan). Dulbecco's modified Eagle's medium (DMEM) was purchased from Gibco (USA). High-performance liquid chromatography (HPLC)-grade methanol was purchased from Oceanpak (Sweden). Galactosylceramide (GC) was purchased from Matreya LLC., (Shanghai, China). Other reagents were of analytical grade and distilled water was used in all experiments.

3.2. Synthesis and optimization of MSN

The MSN was prepared according to the modified Stöber method (Wu et al. 2013). Briefly, 0.0061 mol/L CTAB, 0.0118 mol/L sodium hydroxide (NaOH, 2.0 M) and anhydrous ethanol (ethanol/water, 1:8, v/v) were mixed and stirred in 120 mL deionized water for 20 min at 80 °C. Then, 0.0512 mol/L TEOS was added dropwise slowly to the mixture while stirring. After 2 h, the solution was centrifuged at 16,000 rpm to get the material, and it was washed with deionized water and anhydrous ethanol, and vacuum-dried overnight.

The CTAB was removed by solvent extraction (Hua 2001). The obtained material was refluxed at 80 °C with 5.3% hydrochloric acid/anhydrous ethanol (1g:100 mL) for 6 h. After centrifugation at 16,000 rpm, the final product – MSN was washed with deionized water and anhydrous ethanol three times and dried in vacuum overnight.

3.3. Preparation of HCPT-MSN

The solvent adsorption method was used to load MSN with HCPT (Cha et al. 2012). Briefly, 10 mg of MSN was added to 5 mL of a solution of HCPT in N,N-dimethylformamide (2 mg/mL) and the mixture was stirred for 6 h in a sealed and dark environment. The mixture was subsequently centrifuged at 16,000 rpm to collect the precipitate which was vacuum-dried to obtain HCPT-MSN and supernatant which was analyzed using HPLC. The effect of different HCPT/MSN ratios on the drug loading efficiency was investigated.

3.4. Preparation and optimization of HCPT-GC-LMSN

The surface of HCPT-MSN was lipid-coated using the lipid film hydration method (Teng et al. 2013). 0.6 mg/mL cholesterol, 5 mg/mL phospholipids and 0.5 mg/mL HCPT-MSN were dissolved in a mixture of chloroform-anhydrous ethanol (1:1, v/v) and then a phospholipid membrane was obtained from the solution using a rotary evaporator. Next, the membrane was hydrated with 10 mL phosphate-buffered saline (PBS, pH 6.8) and the suspension was sonicated to obtain the HCPT-LMSN.

To optimize the formulation, the central composite design-response surface methodology (CCD-RSM) was used to modulate the preparation technique of HCPT-LMSN (Liu et al. 2017). Based on the results of our previous single-factor investigation, the following four single factors, concentrations of cholesterol (X_1), phospholipid (X_2), and HCPT-MSN (X_3), and temperature (X_4) were chosen with a four-factor and five-level table (30 formulations). After establishing the optimized formulation, GC was linked to the lipid membrane by adding it to the mixture of chloroform-anhydrous ethanol (1:1, v/v) at a 1:3 ratio of CG:phospholipid (mol/mol).

3.5. MSN Characterization

The MSN morphology was observed using scanning electron microscopy (SEM), and the samples were coated with a thin layer of gold by sputtering before testing. The morphological structure of the MSN was examined using transmission electron microscopy (TEM). For TEM imaging, one drop of the sample solution was placed on a copper screen covered with a carbon film and air-dried. The pore properties of the MSN were evaluated using nitrogen adsorption-desorption with a surface and pore size analyzer, and the Brunauer-Emmett-Teller (BET) and Barrett-Joyner-Halenda (BJH) results were calculated using the Random software. The X-ray diffractometer (XRD) pattern of the samples was obtained using an XRD equipped with a CuKα radiation source at a tube voltage and current of 40 kV and 100 mA, respectively and scanning range (2θ) from 0° to 10°. The particle size, zeta-potential, and polydispersity index (PDI) of the MSN were determined using a laser particle size analyzer, and the particle size of the HCPT-GC-LMSN was determined using a Marvin particle size analyzer.

3.6. Determination of drug loading and encapsulation efficiency

The results of drug loading of HCPT-MSN and encapsulation efficiency (EE) of HCPT-GC-LMSN were determined using HPLC at 384 nm. A reversed phase C_{18} analytical column was used to separate the HCPT at a flow rate of 0.6 mL/min and an injection volume of 20 µL. The mobile phase consisted of 60% methanol and 40% PBS (pH 5.0, v/v).

3.7. In vitro drug release

The *in vitro* drug release assay of HCPT-GC-LMSN was carried out using dynamic dialysis (Zhang et al. 2008). To determine the accumulative release degree of HCPT-GC-LMSN in normal body fluid environment and tumor conditions, PBS containing 1 % sodium dodecyl sulfate (SDS) was used as the release medium under two different simulation conditions: pH 7.4 at 37±1 °C and pH 5.8 at 42±1 °C. Briefly, 2 mL of HCPT-GC-LMSN and an equal dose of HCPT solution were transferred to separate dialysis bags (the cut off is 8000-10000), which were placed in the release medium (30 mL) respectively with stirring speed of 100±1 rpm. Samples of the solution (5 mL) were collected from release medium at 0, 15, and 30 min, and 1, 2, 4, 6, 8, 10, 12, 24, and 36 h and passed through a 0.45 µm microporous membrane filter. In addition, the same volume of fresh release medium (5 mL) was added to the release medium. The concentrations of HCPT were determined using HPLC, and the accumulative release degree was calculated based on the following equation:

$$Q\frac{vc_i + \int_{i=1}^{n-1} v_i c_{i-1}}{M} * 100$$

(Q represents the cumulative release rate V represents the volume of release medium, Ci represents the concentrations of HCPT at i-th sampling time, Vi represents the sampling volume at i-th sampling time, and M represents the whole concentrations of HCPT). Similarly, the accumulative release degree of equal amount of HCPT was researched under pH 7.4 at 37±1 °C condition to compare the impact of lipid coated particles and uncoated drug.

3.8. CCK-8 cell viability assay

The cell viability was measured using a CCK-8 assay (Li et al. 2017). $HepG_2$ cells were seeded into 96-well plates at a density of 1×10^4 cells/well and grown in DMEM-HG containing 10 % fetal bovine serum at 37 °C for 24 h. The cells were divided into two groups: HCPT and HCPT-GC-LMSN. In each group, the cells were treated with HCPT at 2.5, 5, 10, 20, and 40 µg/mL for 24, 48, and 72 h. After treatment with HCPT, the cells were incubated with 10 µL CCK-8 solution for 1 h at 37 °C, and then the optical density (OD) was determined using a microplate reader. The half-maximal inhibitory concentration (IC_{50}) was analyzed using the statistical package for the social sciences (SPSS) software.

3.9. Data analysis

All the data were analyzed after determination of the effects of the formulations. The statistical analysis was performed using the statistical package for the social sciences (SPSS) version 17.0 statistical software. The data are expressed as the mean±standard deviation (SD) and $P < 0.05$ was considered statistically significant.

Acknowledgments: This study was supported by the National Natural Science Foundation of China [#1 Grant number 81673608]; Guangdong Province Science and Technology Project #2 [Grant numbers 2014A020212685 and 2015A020211034], and the Guangzhou Science and Technology Project [#3, Grant number 201707010155]. We appreciate all the staff of the Pharmacy Laboratory of Guangdong Pharmaceutical University.

Conflicts of interest: None declared.

References

Alvarez-Berríos MP, Vivero-Escoto JL (2016) In vitro evaluation of folic acid-conjugated redox-responsive mesoporous silica nanoparticles for the delivery of cisplatin. Int J Nanomed 11: 6251-6265.

Cha KH, Cho KJ, Kim MS, Kim JS, Park HJ, Park J, Cho W, Park JS, Hwang SJ (2012) Enhancement of the dissolution rate and bioavailability of fenofibrate by a melt-adsorption method using supercritical carbon dioxide. Int J Nanomed 7: 5565-5575.

Dai L, CaoX, Liu KF, Li CX, Zhang GF, Deng LH, Si CL, He J, Lei JD (2015) Self-assembled targeted folate-conjugated eight-arm-polyethylene glycol-betulinic acid nanoparticles for co-delivery of anticancer drugs. J Mater Chem B 3: 3754-3766.

Dengler EC, Liu J, Kerwin A, Torres S, Olcott CM, Bowman BN, Armijo L, Gentry K, Wilkerson J, Wallace J, Jiang X, Carnes EC, Brinker CJ, Milligan ED (2013) Mesoporous silica-supported lipid bilayers (protocells) for DNA cargo delivery to the spinal cord. J Control Release 168: 209-224.

Dutta M, Basu JK (2012) Statistical optimization for the adsorption of acid fuchsin onto the surface of carbon alumina composite pellet: an application of response surface methodology. J Environ Sci Technol 5: 42-53.

Fan ZX, Liu GH, Li Y, Ma JY, Lin JY, Guo FQ, Hou ZQ, Xie LY (2016) Self-assembly of the active lactone form of a camptothecin-phospholipid complex for sustained nuclear drug delivery. RSC Adv 6: 82949-82960.

Fu YR, Yi ZJ, Yan YR, Qiu ZY (2006) Hydroxycamptothecin-induced apoptosis in hepatoma SMMC-7721 cells and the role of mitochondrial pathway. Mitochondrion 6: 211-217.

Gao Y, Chen Y, Ji X, He X, Yin Q, Zhang Z, Shi J, Li Y (2011) Controlled intracellular release of doxorubicin in multidrug-resistant cancer cells by tuning the shell-pore sizes of mesoporous silica nanoparticles. ACS Nano 5: 9788-9798.

Heikkilä T, Salonen J, Tuura J, Kumar N, Salmi T, Murzin DY, Hamdy MS, Mul G, Laitinen L, Kaukonen AM, Hirvonen J, Lehto V (2007) Evaluation of mesoporous TCPSi, MCM-41, SBA-15, and TUD-1 materials as API carriers for oral drug delivery. Drug Deliv 14: 337-347.

Hsiao JK, Tsai CP, Chung TH, Hung Y, Yao M, Liu HM, Mou CY, Yang CS, Chen YC, Huang DM (2008) Mesoporous silica nanoparticles as a delivery system of gadolinium for effective human stem cell tracking. Small 4: 1445-1452.

Hua ZL, Shi JL, Wang L, Zhang WH (2001) Preparation of mesoporous silica films on a glass slide: surfactant template removal by solvent extraction. J Non-Cryst Solids 292: 177-183.

Huang C, Wu H, Li R (2012) Improving lipid production from bagasse hydrolysate with Trichosporon fermentans by response surface methodology. New Biotechnol 29: 372-378.

Huang PK, Lin SX, Tsai MJ, Leong MK, Lin SR, Kankala RK, Lee CH, Weng CF (2017) Encapsulation of 16-hydroxycleroda-3,13-dine-16,15-olide in mesoporous silica nanoparticles as a natural dipeptidyl peptidase-4 inhibitor potentiated hypoglycemia in diabetic mice. Nanomaterials (Basel) 7: 112-129.

Jaxel C, Kohn KW, Wani MC, Wall ME, Pommier Y (1989) Structure-activity study of the actions of camptothecin derivatives on mammalian topoisomerase I: evidence for a specific receptor site and a relation to antitumor activity. Cancer Res 49: 1465-1469.

Lee MH, J. H. Han, P. S. Kwon, S. Bhuniya, J. Y. Kim, J. L. Sessler, C. Kang, J. S. Kim.2012. Hepatocyte-targeting single galactose-appended naphthalimide: a tool for intracellular thiol imaging in vivo. J Am Chem Soc 134: 1316-1322.

Li H, Yu H, Zhu C, Hu J, Zhang F, Yang D (2016) Cisplatin and doxorubicin dual-loaded mesoporous silica nanoparticles for controlled drug delivery. RSC Adv 6: 94160-94169.

Li X, Chen H, Sun Y, Dai J, Wang S, Wang J, Yan L (2017) Hydroxycamptothecin prevents intraarticular scar adhesion by activating the PERK signal pathway. Eur J Pharmacol 810: 36-43.

Li Z, Barnes JC, Bosoy A, Stoddart JF, Zink JI (2012) Mesoporous silica nanoparticles in biomedical applications. Chem Soc Rev 41: 2590-2605.

Li ZK, Xi HA, Qian XF (2003) Morphological control of mesoporous silica in a base condition. J Inorg Mater 5: 1102-1106.

Lin JY, Li Y, Wu HJ, Yang XR, Li YX, Ye SF, Hou ZQ, Lin CJ (2015) Tumor-targeted co-delivery of mitomycin C and 10-hydroxycamptothecin via micellar nanocarriers for enhanced anticancer efficacy. RSC Adv 5: 23022-23033.

Liong M, Lu J, Kovochich M, Xia T, Ruehm SG, Nel AE, Tamanoi F, Zink JI (2008) Multifunctional inorganic nanoparticles for imaging, targeting, and drug delivery. ACS Nano 2: 889-896.

Liu B, He D, Wu J, Sun Q, Zhang M, Tan Q, Li, J, Zhang Y (2017) Catan-ionic hybrid lipidic nano-carriers for enhanced bioavailability and anti-tumor efficacy of chemodrugs. Oncotarget 8: 30922-30932.

Liu HM, Wu SH, Lu CW, Yao M, Hsiao JK, Hung Y, Lin YS, Mou CY, Yang CS, Huang DM, Chen YC (2008) Mesoporous silica nanoparticles improve magnetic labeling efficiency in human stem cells. Small 4: 619-626.

Liu J, Stace-Naughton A, Jiang X, Brinker CJ (2009) Porous nanoparticle supported lipid bilayers (protocells) as delivery vehicles. J Am Chem Soc 131: 1354-1355.

Lu J, Liong M, Li Z, Zink JI, Tamanoi F (2010) Biocompatibility, biodistribution, and drug-delivery efficiency of mesoporous silica nanoparticles for cancer therapy in animals. Small 6: 1794-1805.

Lv Y, Li J, Chen H, Bai Y, Zhang L (2017) Glycyrrhetinic acid-functionalized mesoporous silica nanoparticles as hepatocellular carcinoma-targeted drug carrier. Int J Nanomedicine 12: 4361-4370.

Mudakaci RJ, Raichur AM, Chakravortty D (2014) Lipid-coated mesoporous silica nanoparticles as an oral delivery system for targeting and treatment of intravacuolar Salmonella infections. RSC Adv 4: 61160-61166.

O'Leary J, Muggia FM (1998) Camptothecins: a review of their development and schedules of administration. Eur. J. Cancer 34: 1500-1508.

Pu X, Sun J, Wang Y, WangY, Liu X, Zhang P, Tang X, Pan W, Han J, He Z (2009) Development of a chemically stable 10-hydroxycamptothecin nanosuspensions. Int J Pharm 379: 167-173.

Qiu Y, Wu C, Jiang J, Hao J, Zhao Y, Xu J, Yu T, Ji P (2017) Lipid-coated hollow mesoporous silica nanospheres for co-delivery of doxorubicin and paclitaxel: Preparation, sustained release, cellular uptake, and pharmacokinetics. Mater Sci Eng C Mater Biol Appl 71: 835-843.

Qu F, Zhu G, Huang S, Li S, Sun J, Zhang D, Qui S (2006) Controlled release of Captopril by regulating the pore size and morphology of ordered mesoporous silica. Microporous Mesoporous Mater 92: 1-9.

Qu Y, Li H, Li A, Ma F, Zhou J (2011) Identification and characterization of *Leucobacter* sp. N-4 for Ni (II) biosorption by response surface methodology. J Hazard Mater 190: 869-875.

Sing KSW (1985) Reporting physisorption data for gas/solid systems with special reference to the determination of surface area and porosity (Recommendations 1984). Pure Appl Chem 57: 603-619.

Slowing II, Trewyn BG, Lin VSY (2007) Mesoporous silica nanoparticles for intracellular delivery of membrane-impermeable proteins. J Am Chem Soc 129: 8845-8849.

Song C, Zhang SB, Zhou Q, Shi L, Du LY, Zhi DF, Zhao YN, Zhen YH, Zhao DF (2017) Bifunctional cationic solid lipid nanoparticles of β-NaYF4: Yb, Er upconversion nanoparticles coated with a lipid for bioimaging and gene delivery. RSC Adv 7, 26633-26639.

Teng IT, Chang YJ, Wang LS, Lu HY, Wu LC, Yang CM, Chiu CC, Yang CH, Hsu SL Ho JA (2013) Phospholipid-functionalized mesoporous silica nanocarriers for selective photodynamic therapy of cancer. Biomaterials 34: 7462-7470.

Tu J, Du G, Nejadnik MR, Mönkäre J, van der Maaden K, Bomans PHH, Sommerdijk NAJM, Slütter B, Jiskoot W, Bouwstra JA, Kros A (2017) Mesoporous silica nanoparticle-coated microneedle arrays for intradermal antigen delivery. Pharm Res 34: 1693-1706.

Vallet-Regí M, Balas, F Arcos D (2007) Mesoporous materials for drug delivery. Angew Chem Int Ed Engl 46: 7548-7558.

Vittal R, Kim KJ, Gomathi H, Yegnaraman V (2008) CTAB-promoted prussian blue-modified electrode and its cation transport characteristics for K^+, Na^+, Li^+, and NH_4^+ ions. J Phys Chem B 112: 1149-1156.

Vivero-Escoto JL, Slowing II, Trewyn BG, Lin VS (2010) Mesoporous silica nanoparticles for intracellular controlled drug delivery. Small 6: 1952-1967.

Wang J, Wang R, Li LB (2009) Preparation and properties of hydroxycamptothecin-loaded nanoparticles made of amphiphilic copolymer and normal polymer. J Colloid Interface Sci 336: 808-813.

Wei W, Yue ZG, Qu JB, Yue H, Su ZG, Ma GH (2010) Galactosylated nanocrystallites of insoluble anticancer drug for liver-targeting therapy: an in vitro evaluation. Nanomedicine 5: 589-596.

Wu SH, Mou CY, Lin HP (2013) Synthesis of mesoporous silica nanoparticles. Chem Soc Rev 42: 3862-3875.

Wu X, Wang Z, Zhu D, Zong S, Yang L, Zhong Y, Cui Y (2013) pH and thermo dual-stimuli-responsive drug carrier based on mesoporous silica nanoparticles encapsulated in a copolymer–lipid bilayer. *A*CS Appl Mater Interfaces 5: 10895-10903.

Yamada Y, Yano K (2006) Synthesis of monodispersed super-microporous/mesoporous silica spheres with diameters in the low submicron range. Microporous Mesoporous Mater 93: 190-198.

Yanes RE, Tamanoi F (2012) Development of mesoporous silica nanomaterials as a vehicle for anticancer drug delivery. Ther Deliv 3: 389-404.

Yang X, Wu S, Wang Y, Li Y, Chang D, Luo Y, Ye S, Hou Z (2014) Evaluation of self-assembled HCPT-loaded PEG-b-PLA nanoparticles by comparing with HCPT-loaded PLA nanoparticles. Nanoscale Res Lett 9: 687-695.

Yano K, Fukushima F (2004) Synthesis of mono-dispersed mesoporous silica spheres with highly ordered hexagonal regularity using conventional alkyltrimethylammonium halide as a surfactant. J Mater Chem 14: 1579-1584.

Zhang X, Pan W, Gan L, Zhu C, Gan Y, Nie S (2008) Preparation of a dispersible PEGylate nanostructured lipid carriers (NLC) loaded with 10-hydroxycamptothecin by spray-drying. Chem Pharm Bull (Tokyo) 56: 1645-1650.

Zhao X, Jiang R, Zu Y, Wang Y, Zhao Q, Zu, Zhao D, Wang M, Sun Z (2012) Process optimization studies of 10-hydroxycamptothecin (HCPT)-loaded folate-conjugated chitosan nanoparticles by SAS-ionic crosslink combination using response surface methodology (RSM). Appl. Surf. Sci 258: 2000-2005.